

# Effects of Magnet Shape on Torque Capability of Surface-Mounted Permanent Magnet Machine for Servo Applications

Yu Zeng<sup>ID</sup>, Student Member, IEEE, Ming Cheng<sup>ID</sup>, Fellow, IEEE, Guohai Liu<sup>ID</sup>, Senior Member, IEEE, and Wenxiang Zhao<sup>ID</sup>, Senior Member, IEEE

**Abstract**—This paper proposes three new methods to improve torque capability for the surface-mounted permanent magnet machine in a servo system. The key to the proposed methods is to explore various magnet shape designs via sufficient attempts of harmonic combinations. Such techniques serve to avoid a significant drop in the average torque when reducing the torque ripple. The effect of analytical harmonic compensation on output torques is investigated by the finite-element method, and diverse torques are evaluated by a predefined objective function, which as an evaluation criterion of the torque performance is established. Comparisons of the proposed and the existing methods are carried out, showing the higher average torque and the lower torque ripple of the proposed method. Finally, a prototype machine designed with one of the proposed methods is fabricated and tested for validation.

**Index Terms**—Air gaps, electromagnetic fields, finite-element analysis, harmonic analysis, harmonic distortion, permanent magnet (PM) machines, rotors, torque.

## NOMENCLATURE

$a_{2n-1}$ , $b_{2n-1}$ , and $c_{2n-1}$ ( $n > 0$ )	Amplitudes of $(2n-1)$ th harmonic in sine harmonic compensation (SHC), inverse cosine harmonic compensation (ICHc), and tangent harmonic compensation (THC) functions.
$A_{2n-1}$ , $B_{2n-1}$ , and $C_{2n-1}$ ( $n > 0$ )	Amplitudes of $(2n-1)$ th harmonic in SHC, ICHC, and THC methods.
$B$	Air-gap flux density.

Manuscript received August 25, 2018; revised November 27, 2018, January 27, 2019, and March 7, 2019; accepted March 24, 2019. Date of publication April 15, 2019; date of current version December 9, 2019. This work was supported in part by the State Key Laboratory of Air-Conditioning Equipment and System Energy Conservation under Project ACSKL2018KT08 and in part by the Scientific Research Foundation of Graduate School of Southeast University under Project YBPY1878. (Corresponding author: Ming Cheng.)

Y. Zeng and M. Cheng are with the School of Electrical Engineering, Southeast University, Nanjing 210096, China (e-mail: zengyu92@foxmail.com; mcheng@seu.edu.cn).

G. Liu and W. Zhao are with the School of Electrical and Information Engineering and the Jiangsu Key Laboratory of Drive and Intelligent Control for Electric Vehicle, Jiangsu University, Zhenjiang 212013, China (e-mail: ghliu@ujs.edu.cn; zwx@ujs.edu.cn).

Color versions of one or more of the figures in this paper are available online at <http://ieeexplore.ieee.org>.

Digital Object Identifier 10.1109/TIE.2019.2910025

$B'$	Air-gap flux density under harmonic compensation.
$B_r$	Magnet remanence of permanent magnet (PM).
$h_m$ and $h'$	PM thickness of original machine.
$l$	Variation of PM thickness.
$M$	Total length of PM and air-gap.
$T_{\text{orig\_avg}}$ and $T_{\text{orig\_ripple}}$	Harmonic compensation function.
$T_{\text{avg}}$ , $T_{\text{max}}$ , $T_{\text{min}}$ , and $T_{\text{ripple}}$	Average torque and torque ripple of original machines.
$W_a$ and $W_r$	Average torque, maximum torque, minimum torque, and torque ripple of shaped machines.
$q$	Weights of average torque and torque ripple.
$S_p$	Number of slots per pole per phase.
$\alpha_p$	Shaped arc.
$\omega$	Pole-arc coefficient.
$\theta$	Shaped period.
$\theta_m$	Shaped arc angle.
$\tau_p$	Maximum value of shaped arc angle.
$\delta$	Pole pitch.
$\delta_{\text{air}}$	Air-gap length.
$\delta_q$	Air-gap length of the original machine.
$\Delta m$	Maximum air-gap length.
$\Delta m_a$ and $\Delta m_b$	A variable to keep the maximum PM thickness or minimum air-gap length constant in harmonic compensation function.
	A variable to keep the maximum PM thickness or minimum air-gap length constant in SHC and ICHC methods.

## I. INTRODUCTION

INCE surface-mounted permanent magnet (SPM) brushless machines offer high torque density, high efficiency, and the excellent dynamic performance, they have made the technology attractive to researchers and shown as a promising alternative to the conventional dc–ac machines in the servo system [1]–[3]. High-performance PM servo machines are expected to provide high average torque and low torque ripple, and hence, the torque ripple reduction and average torque

improvement have received increasing attention [4]–[14]. The phenomenon of the average torque decrement is a prevalent obstacle that PM machines usually experience when a large number of literatures focus on the torque ripple reduction. Furthermore, although there have been various methods to enhance the average torque, they suffer from the torque ripple increment. Therefore, finding a method for the torque ripple reduction without a drop in the average torque, emerges as a catching and challenging task.

To address the problem of torque ripple, the cogging torque minimization or the back electromotive force (EMF) optimization becomes a good candidate. In [4], an approach for shaping the stator geometry of a PM machine toward a desired cogging torque was reported. The output power measurement indicated an acceptably small power ripple of <8%, while the torque density was inevitably reduced due to the increment of the equivalent air-gap length. A conventional method of total torque ripple reduction by magnets shifting was proposed in [5]. The result showed that the torque ripple is reduced by 5–20.2% with a total torque loss of 5–7%. Du and Lipo [6] proposed a new design method of arranging rotor segments in the axial direction to improve the PM utilization and reduce the torque ripple. Although the torque per magnet weight is improved by 15%, 9% torque decrement of the interior PM (IPM) machine is achieved. Additionally, research into magnet or rotor shape to reduce the torque ripple in IPM and SPM machines has been intensively conducted [7], [8]. Asymmetric rotor shape under certain load condition was investigated in [7], making the air-gap flux density sinusoidal, but the average torque decayed by 6%. In [8], a new method of PM shape optimization was proposed to reduce the harmonics of the magnetic field, whereas 6.2% decline in average torque was generated. Therefore, a technique that can reduce the torque ripple but avoid a significant drop in the average torque is highly desired.

On the other hand, many methods have been proposed to increase the average torque, and especially harmonic injection has become a popular method that has many applications. A sinusoidal shaping method with the third harmonic injection was discussed in SPM machines, improving the average torque [9]. However, the optimal amplitude of the third harmonic was not investigated. The optimal third harmonic under a constant maximum PM thickness was deduced in [10] and [11], showing that the optimal amplitude of the third harmonic is 1/6 of the fundamental component. Based on this conclusion, the fifth- and seventh-order harmonic injections were further derived in [12]. However, the conclusions and employed methods in [10]–[12] had limitations. The injected harmonics were multiplied by one parameter to meet the constraint of remaining a constant maximum PM thickness, which results in distorted amplitudes of the injected harmonics, and hence, the variation ranges of harmonic combinations and PM topologies were restricted. Moreover, the results fail to serve as a general theory for different SPM machines since the torque ripple can be unacceptable when gaining the maximum average torque. In [13], the PM shape utilizing analytical feedback function was proposed for the torque quality enhancement. This approach, characterized by involving a variety of PM topologies, however, adds the air-gap flux density

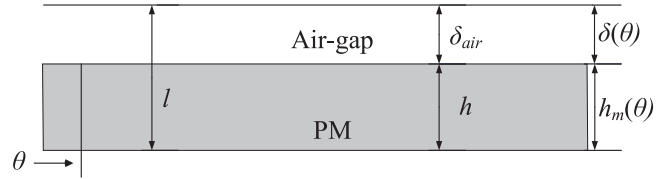


**Fig. 1.** Simplified air-gap and the PM model to explain air-gap flux density production.

harmonics of the original machine to the shaped function. It means that the amplitudes and orders of injected harmonics are changed, and then causing the mismatch between the injected harmonics and the PM topologies. Besides, the shaped function is over-complicated. With regard to the inverse cosine shaping method, a third harmonic was introduced to IPM machines for average torque improvement [14], but it suffers from the same drawbacks in [10]–[12].

In this paper, three magnet shaping methods, including sine harmonic compensation (SHC), inverse cosine harmonic compensation (ICHC), and tangent harmonic compensation (THC), are proposed to improve torque quality. The proposed methods seek to reduce torque ripple and avoid a significant drop in the average torque, focusing on exploring various harmonic combinations and different PM topologies to produce diverse output torques. An output-torques-based database is built to evaluate the torque quality via a predefined objective function. Finally, the optimal torque is determined. Owing to a sufficient database, the proposed methods show universality in magnet shape design for different SPM machines.

This paper is organized as follows. In Section II, the detailed derivation and main idea of the proposed methods will be illustrated. In Section III, the optimization procedures of a 9-slot/6-pole machine will be described. The electromagnetic performance of three proposed methods will be predicted in Section IV, and comparisons between the proposed and existing methods will also be carried out. In Section V, a 9-slot/6-pole SHC prototype will be assessed experimentally to validate the theoretical analysis. Finally, Section VI concludes this paper.

## II. MAGNET SHAPE WITH HARMONIC COMPENSATION

Fig. 1 shows the simplified air-gap and PM model to explain the air-gap flux density production. Ignoring the slot opening, the teeth effect, the flux saturation, and other parameters, the air-gap flux density of an SPM machine with radial magnetization can be expressed ideally as [15]

$$B(\theta) = \frac{h_m(\theta)}{l} B_r. \quad (1)$$

However, the air-gap flux density is influenced by various variables such as the slot opening, the teeth effect, the ratio of pole arc to pole pitch, the flux saturation, and so on [11], thus distorting the practical air-gap flux density. Therefore, some techniques should be employed to compensate for negative impacts, and the harmonic injection, in particular, becomes a good candidate. The expression of the air-gap flux density under the

harmonic compensation is given by

$$B(\theta) + M = B'(\theta). \quad (2)$$

From (1) and (2), the practical PM thickness  $h'_m(\theta)$  is derived as

$$h'_m(\theta) = h_m(\theta) + \frac{l}{B_r} M \quad (3)$$

where the general PM thickness  $h_m(\theta)$  is a constant  $h$  because the tile PM is usually used.

In addition, there is a constraint condition to remain maximum PM thickness the same before and after the harmonic compensation, as characterized by

$$h'_m(\theta)_{\max} = h. \quad (4)$$

Since the total air-gap length  $l$ , which contains the PM thickness  $h$  and the air-gap length  $\delta_{\text{air}}$ , keeps constant as shown in Fig. 1, an equivalent constraint condition can be derived from (4), namely

$$\delta(\theta)_{\min} = \delta_{\text{air}}. \quad (5)$$

### A. Sine Harmonic Compensation

The SHC function with all rank harmonics is introduced to the PM for torque improvement, while the constraint condition (4) should be satisfied, and hence, the harmonic compensation function is given by

$$M = \sum_{n=1}^{\infty} a_{2n-1} \sin[(2n-1)\omega\theta] - \Delta m \quad n = 1, 2, 3, \dots \quad (6)$$

When the value of  $n$  is unity, (6) becomes a very common method to generate the sinusoidal air-gap flux density. In addition, the third, fifth, seventh harmonics, and those with higher orders are utilized for increasing the average torque. The SHC method proposes a key parameter  $\Delta m$ , which is the maximum value of the first term in (6), varying with different harmonic orders and their amplitudes, consequently extending the investigation range of PM topologies. By contrast, existing methods multiplied by one parameter to meet the constraint condition (4) that actually distorts the amplitudes of the injected harmonics, resulting in a limited conclusion even though the optimal amplitudes of the third, fifth, and seventh harmonics are theoretically derived [10]–[12]. Further explanations of the proposed methods will be given in the following analysis.

Based on the characteristic of the SHC function, the following variables are defined

$$\begin{cases} \Delta m_a = l\Delta m/B_r \\ \omega = p\alpha_p = pS_p/\tau_p \\ A_{2n-1} = la_{2n-1}/B_r \end{cases} \quad (7)$$

From (3), (6), and (7), the shaped PM can be described as

$$h'_m(\theta) = h_m(\theta) - \Delta m_a(A_{2n-1}) + \sum_{n=1}^{\infty} A_{2n-1} \sin \left[ (2n-1) \frac{S_p}{\tau_p} p\theta \right] \quad (8)$$

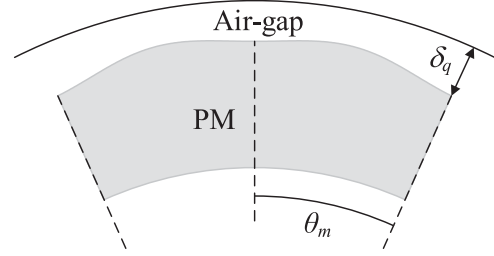


Fig. 2. Variation of Air-gap length with shaped arc angle  $\theta$ .

where the ratio of the shaped arc  $S_p$  to the pole pitch  $\tau_p$  determines the pole-arc coefficient, which is the shaped period of the SHC function. The third term in (8) presents the variation of the PM thickness, while  $\Delta m_a$  is the maximum value of the third term to meet the requirement of (4).

### B. Inverse Cosine Harmonic Compensation

The ICHC function with various harmonics is newly developed, which is given by

$$M = - \left( \frac{\delta_{\text{air}}}{\sum_{n=1}^{\infty} b_{2n-1} \cos[(2n-1)\omega\theta]} + \Delta m \right) \quad n = 1, 2, 3, \dots \quad (9)$$

The ICHC method operates on the air-gap length to produce the desired air-gap flux density. Furthermore, (9) offers a key parameter  $\Delta m$  to vary with various harmonic orders and their amplitudes, that is, satisfying the constraint condition (5).

From the perspective of the characteristic of the ICHC function, the following variables can be defined

$$\begin{cases} \Delta m_b = l\Delta m/B_r \\ \omega = \frac{\arccos(\delta_{\text{air}}/\delta_q)}{\theta_m} \\ B_{2n-1} = B_r b_{2n-1}/l \end{cases} \quad (10)$$

From (3), (9), and (10), the shaped function can be rewritten as

$$h'_m(\theta) = h_m(\theta) - \Delta m_b(B_{2n-1}) - \frac{\delta_{\text{air}}}{\sum_{n=1}^{\infty} B_{2n-1} \cos[(2n-1) \frac{\arccos(\delta_{\text{air}}/\delta_q)}{\theta_m} \theta]}. \quad (11)$$

Like the SHC method,  $\Delta m_b$  is the maximum value of the third term in (11) to follow the demand of (5). However, the identification of  $\omega$  is supposed to pay more attention.

The fundamental harmonic is the first priority, and then the air-gap length function is given by

$$\delta(\theta) = \frac{\delta_{\text{air}}}{\cos(\omega\theta)}. \quad (12)$$

As seen from (12) that the minimum air-gap length is a constant  $\delta_{\text{air}}$ , implying  $\Delta m_b$  is zero. The maximum air-gap length  $\delta_q$  is generated by the maximum angle  $\theta_m$  as shown in Fig. 2.

Then, (12) can be deduced as

$$\delta(\theta_m) = \delta_q = \frac{\delta_{\text{air}}}{\cos(\omega\theta_m)}. \quad (13)$$

For an easy transformation, (13) is rewritten as

$$\omega = \frac{\arccos(\frac{\delta_{\text{air}}}{\delta_q})}{\theta_m}. \quad (14)$$

It is worth noting that  $\omega$  will remain the same if the third, fifth, and those with higher order harmonics are injected into the ICHC function.

### C. Tangent Harmonic Compensation

The SHC and ICHC methods adopt a key parameter  $\Delta m$  to manipulate different harmonic injection, thus providing a better torque performance than that of existing methods. However, there are two drawbacks for the two methods due to the presence of  $\Delta m$ . On the one hand, the mapping relation between  $\Delta m$  and various harmonics cannot be analytically deduced because the number of variables is more than that of the constraint conditions. On the other hand, the workload is relatively large, since every harmonic combination needs to calculate a  $\Delta m$  and analyze the corresponding PM topology by finite-element (FE) method (FEM). Consequently, determining if the method can keep the maximum PM thickness constant under various harmonics compensation should be an essential goal.

The THC method is newly considered, which is expressed by

$$\delta(\theta) = |\tan(\omega\theta)| = \left| \frac{\sin(\omega\theta)}{\cos(\omega\theta)} \right| \quad (15)$$

where  $n$  of unity is taken into account. Like the derivation from (12) to (14),  $\omega$  can be calculated by

$$\omega = \frac{\arctan(\delta_q - \delta_{\text{air}})}{\theta_m}. \quad (16)$$

Then, the THC function is characterized by

$$M = - \left| \frac{\sin(\omega\theta)}{\sum_{n=1}^{\infty} c_{2n-1} \cos[(2n-1)\omega\theta]} \right| \quad n = 1, 2, 3, \dots \quad (17)$$

To simplify the calculation, the amplitudes of compensated harmonics should be

$$C_{2n-1} = B_r c_{2n-1} / l. \quad (18)$$

Substituting (16)–(18) into (3), the shaped function is derived by

$$h'_m(\theta) = h_m(\theta) - \left| \frac{\sin[\frac{\arctan(\delta_q - \delta_{\text{air}})}{\theta_m}\theta]}{\sum_{n=1}^{\infty} C_{2n-1} \cos[(2n-1)\frac{\arctan(\delta_q - \delta_{\text{air}})}{\theta_m}\theta]} \right|. \quad (19)$$

From (19), the maximum PM thickness (namely, the minimum air-gap length) maintains a constant  $h$  when  $\theta$  is selected to be zero. Therefore, the introduction of  $\Delta m$  is no need for the THC method.

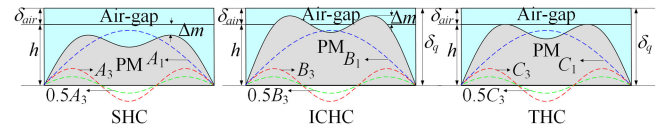


Fig. 3. Graphic illustration of SHC, ICHC, and THC method.

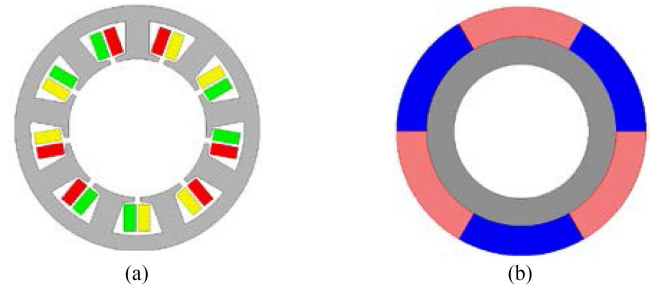


Fig. 4. Topology of 9-slot/6-pole SPM machine. (a) 9-slot stator with three-phase fractional-slot concentrated windings. (b) 6-pole rotor.

TABLE I  
SPECIFICATIONS OF 9-SLOT/6-POLE MACHINE

Design parameters	9-slot/6-pole
Peak current	7.07 A
Number of slot and pole	9, 6
Rated speed	300 rpm
Outer and inner diameters of stator	80 mm, 45 mm
Axial length of stator core	86 mm
Outer and inner diameters of rotor	42 mm, 21 mm
Minimum air-gap length $\delta$	1.5 mm
Maximum thickness of PMs $h$	5.5 mm
Thickness of rotor core	4.5 mm
Slot opening	2 mm
Tooth width	7.8 mm
Magnet remanence $B_r$	1.23 T
Shaped magnet arc	0.0162 rad or 60°
Ratio of shaped arc to pole pitch $S_p/\tau_p$	1

The illustrations of shaped functions of (8), (11), and (19) using graphic manner are given in Fig. 3.

## III. OPTIMIZATION PROCEDURE OF NEWLY SHAPED MACHINES

### A. 9-Slot/6-Pole SPM Machine

A 9-slot/6-pole SPM machine with fractional-slot concentrated windings is introduced to investigate the three harmonic compensation methods. Fig. 4(a) shows the 9-slot stator with three-phase windings, while the original rotor is presented in Fig. 4(b). The design parameters of the two machines are provided in Table I.

### B. Optimization Procedure

The optimization procedure of the SHC, ICHC, and THC methods is presented in Fig. 5, which is divided into five parts (Parts I–V), and the 9-slot/6-pole SHC machine as an example is introduced to explain the detailed content of the corresponding parts.

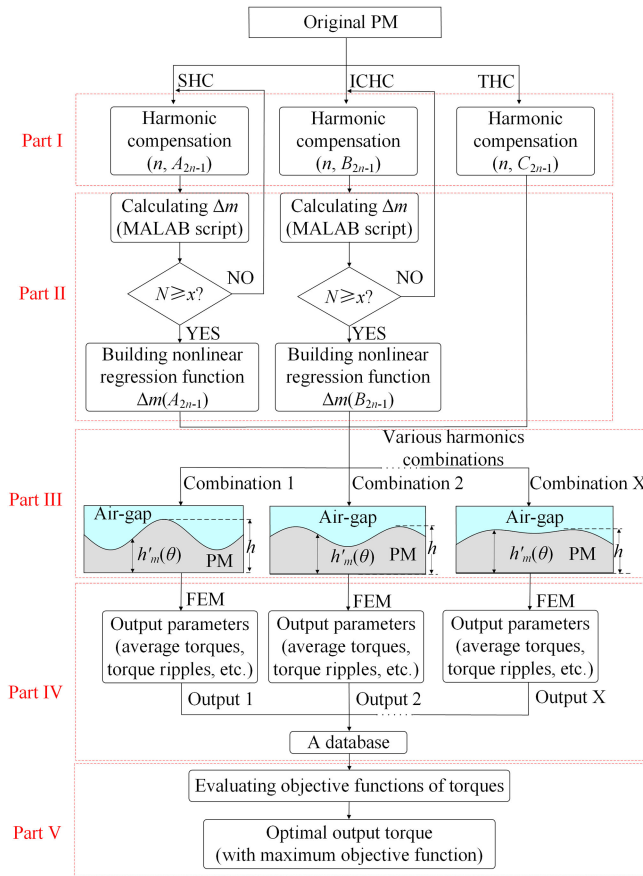


Fig. 5. Optimization procedure of proposed SHC, ICHC, and THC methods.

**1) Part I: Harmonic Injection:** Although  $(2n-1)$ th harmonics as a whole can be utilized for magnet shaping, the ninth harmonic and those with higher orders make minor contributions to torque improvement, which was demonstrated in [13]. Therefore, the fundamental, third, fifth, and seventh harmonics are introduced to improve torque capability.

There are two methods for choosing the coefficients  $A_{(2n-1)}$ . The first way is that  $A_1, A_3, A_5$ , and  $A_7$  are identified at the same time to form a group of harmonic combination. This method suffers from two drawbacks. For one thing, if the numbers of the chosen values for  $A_1, A_3, A_5$ , and  $A_7$  at their changed ranges are all of 100, it will generate  $100^4$  groups of harmonic combination that are hard to be processed. For another thing, the accuracy of the nonlinear regression function is inversely proportional to the number of variables. Four variables ( $A_1, A_3, A_5$ , and  $A_7$ ) indicate that the nonlinear regression function  $\Delta m_a$  ( $A_{2n-1}$ ) is hard to be obtained.

The other method is to optimize  $A_1, A_3, A_5$ , and  $A_7$  one by one. When the numbers of  $A_1, A_3, A_5$ , and  $A_7$  at their changed ranges are all of 100, only 400 groups of harmonic combination need to be considered in this manner, which brings about the accurately nonlinear regression function due to the single variable and the relatively small data to be assessed, thus being employed in SHC, ICHC, and THC methods.

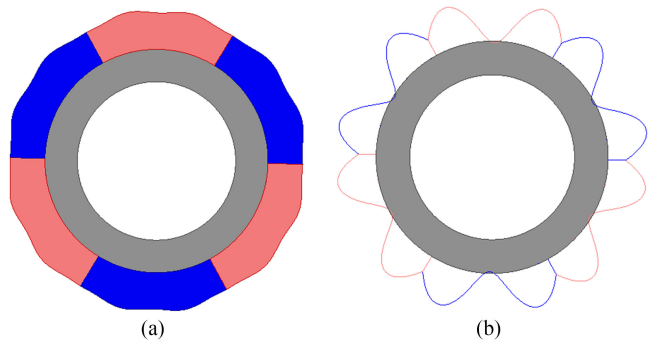


Fig. 6. PM topologies. (a) Normal PM ( $A_3 = 0.1$ ). (b) Abnormal PM ( $A_3 = 2.86$ ).

The steps of how to choose the coefficient  $A_{(2n-1)}$  are given as follows.

1) *Changed range of  $A_{(2n-1)}$ :* The constraint condition of the changed range for  $A_{(2n-1)}$  is that the minimum PM thickness should be larger than zero as shown in (20). For instance, the normal PM topology ( $A_3 = 0.1$ ) is pictured by Fig. 6(a), while the abnormal PM topology is given by Fig. 6(b), which results from the minimum PM thickness of minus, as well as the overlarge coefficient of  $A_3$  (2.86). Therefore, the changed range of  $A_{(2n-1)}$  is limited by (20).

$$h'_m(\theta)_{\min} > 0. \quad (20)$$

2) *Number of  $A_{(2n-1)}$ :* The more number of  $A_{(2n-1)}$  indicates a better solution accuracy. However, the increased number of  $A_3$  brings about the heavy workload in data process and FEM simulation. Generally, 100 values of a variable are recommended. If the changed range of  $A_{(2n-1)}$  is  $-0.5-0.5$ , the arithmetic progression of  $[-0.49, -0.48, -0.47, \dots, 0, 0.01, 0.02, \dots, 0.49, 0.5]$  as the coefficients of  $A_{(2n-1)}$  are chosen.

3) *Harmonic combination:* As seen from (8) that there are only two variables  $\Delta m_a$  and  $A_{2n-1}$ , while  $h, p, l, B_r, S_p/\tau_p$  are listed in Table I. Then, the shaped function with the fundamental harmonic injection  $A_1$  is derived as

$$h'_m(\theta) = 5.5 - \Delta m_a(A_1) + A_1 \sin(3p\theta). \quad (21)$$

If the fundamental harmonic is determined as 0.592, the shaped function with third harmonic  $A_3$  is given by

$$h'_m(\theta) = 5.5 - \Delta m_a(A_3) + 0.592 \sin(3p\theta) + A_3 \sin(3 \times 3\theta). \quad (22)$$

When the fifth harmonic  $A_5$  is injected into the shaped function under the third harmonic  $A_3$  of  $-0.0892$  (optimization process as shown in Part IV), the expression is

$$\begin{aligned} h'_m(\theta) = & 5.5 - \Delta m_a(A_5) + 0.592 \sin(3p\theta) \\ & - 0.0892 \sin(3 \times 3\theta) + A_5 \sin(5 \times 3\theta). \end{aligned} \quad (23)$$

If  $A_5$  is  $-0.197$  (optimization process as shown in Part IV), a group of harmonic combination of  $A_1 = 0.592$ ,  $A_3 = -0.0892$ , and  $A_5 = -0.197$  is generated and the corresponding shaped function can be employed to draw the PM contour.

The key to describe a PM topology using (21)–(23) is to build the relation between  $\Delta m_a$  and  $A_{2n-1}$ , namely, the expression of  $\Delta m_a(A_{2n-1})$ . Consequently, the establishment of the nonlinear regression function  $\Delta m_a(A_{2n-1})$  should be discussed.

## 2) Part II: Establishment of Nonlinear Regression Function $\Delta m$ :

**Function  $\Delta m$ :** With the injection of different harmonics into the magnet, the maximum PM thickness changes in the SHC and ICHC methods. However, it is expected to remain maximum PM thickness the same before and after the harmonic compensation considering the mechanical operation as seen in (4) and (5). As a result, a key variable  $\Delta m$ , which can adjust the PM thickness should be proposed to maintain the maximum PM thickness  $h'_m(\theta)_{\max}$  the same. Additionally, the THC method characterizing a constant maximum PM thickness, eliminates the necessity of  $\Delta m$ .

The 9-slot/6-pole machine with the fundamental, third and fifth harmonics applying the SHC method as an example is developed to exhibit the establishment of the nonlinear regression function. The calculation of  $\Delta m_a$  is based on (4) and (8), which have two variables  $\Delta m_a$  and  $A_{2n-1}$ . Meanwhile, there is a constraint condition  $h'_m(\theta)_{\max} = h$ . Then, the values of  $\Delta m_a$  can be calculated by the harmonic injection ( $A_{2n-1}$ ).

The calculative process is programmed as a script in the MATLAB software. When harmonics are injected into the compensation function, the MATLAB script will calculate the corresponding  $\Delta m_a$  automatically.  $N$  is a number to count how many times of the injected harmonics. Once the number  $N$  is equal to the preset-value  $x$ , the collected data will be fitted to output a nonlinear regression function  $\Delta m_a(A_{2n-1})$ . A higher value of  $x$  implies more data of  $\Delta m_a(A_{2n-1})$  are collected, producing a more accurate mapping relation between  $\Delta m_a$  and  $A_{2n-1}$ . To account for the fitness between the original data and the regression function,  $R$ -square as the coefficient of multiple determination is introduced. This statistic measures how successful the fit is in explaining the variation of the data. A value closer to unity indicates a better fit. For fitting accuracy,  $R$ -square of all regression functions evaluated in this work is greater than 0.99.

Since the maximum PM thickness keeps a constant under the fundamental harmonic  $A_1$  injection, the value of  $\Delta m_a$  is set to zero as given by

$$\Delta m_a(A_1) = 0. \quad (24)$$

From (22), the mapping relation of  $\Delta m_a$  and the third harmonic  $A_3$  is given as

$$\Delta m_a(A_3) = \begin{cases} 8.062A_3^4 + 11.65A_3^3 + 6.378A_3^2 + 0.653A_3 \\ + 0.471 \quad A_3 \in [-0.5, -0.088] \\ 1.483A_3^4 - 1.443A_3^3 + 0.433A_3^2 + 0.961A_3 \\ + 0.529 \quad A_3 \in [-0.088, 0.5] \end{cases}. \quad (25)$$

**TABLE II**  
OPTIMAL HARMONIC COMBINATIONS OF 9-SLOT/6-POLE SPM MACHINE  
USING SHC, ICHC, AND THC METHODS

	1st	3rd	5th	7th	Objective function
9-slot/6-pole (SHC)	$A_1=0.529$	$A_3=-0.0892$	$A_5=-0.197$	$A_7=0$	0.054
9-slot/6-pole (ICHC)	$B_1=1, \delta_q=5.5$	$B_3=-0.02$	$B_5=-0.04$	$B_7=0$	0.052
9-slot/6-pole (THC)	$C_1=1, \delta_q=2.71$	$C_3=0.68$	$C_5=0$	$C_7=0.012$	0.034

Similarly, based on (23),  $\Delta m_a(A_5)$  is expressed by

$$\Delta m_a(A_5) = \begin{cases} 1.119A_5^4 + 1.108A_5^3 - 0.344A_5^2 - 0.967A_5 \\ + 0.618 \quad A_5 \in [-0.5, 0.076] \\ 7.889A_5^4 - 11.01A_5^3 + 5.742A_5^2 - 0.383A_5 \\ + 0.553 \quad A_5 \in [0.076, 0.5] \end{cases}. \quad (26)$$

At this point, the shaped function only varies with the shaped arc angle  $\theta$  when injecting different harmonics, and the PM topology can be described.

**3) Part III: Generation of Various PM Topologies:** A group of harmonic combination contains the injected harmonic orders and their amplitudes that can generate a PM topology using (8) or (11) or (19). Table II depicts three groups of harmonic combination that consist of the optimal fundamental, third, fifth, and seventh harmonics of the 9-slot/6-pole SPM machine when employing SHC, ICHC, and THC methods, and meanwhile, their corresponding PM topologies are described in Fig. 7.

**4) Part IV: FE Prediction and Database:** The shaped SHC rotor produced in Part III, is expected to be imported into FE simulation software to analyze its performance, and then acquiring a group of output parameters, that is, the average torque and the torque ripple. If there are  $X$  groups of harmonic combination, it is natural that  $X$  kinds of PM topologies are described and  $X$  groups of output parameters are obtained. Based on these output parameters, a database is established. The output data in the database need to be processed and evaluated to determine the optimal output torque.

**5) Part V: Objective Function and Determination of Optimal Harmonics:** The objective function as an evaluation criterion for the database is established to assess diverse output torques, which is given by

$$\begin{cases} f(T_{\text{avg}}, T_{\text{ripple}}) = W_a \frac{T_{\text{orig\_avg}} - T_{\text{avg}}}{T_{\text{orig\_avg}}} \\ + W_r (T_{\text{orig\_ripple}} - T_{\text{ripple}}) \\ T_{\text{ripple}} = \frac{T_{\max} - T_{\min}}{T_{\text{avg}}} \end{cases} \quad (27)$$

where  $T_{\text{orig\_avg}}$  and  $T_{\text{orig\_ripple}}$  are constants, while  $W_a$  and  $W_r$  are given as  $-0.5$  and  $0.5$ , respectively. A higher value of the objective function indicates a better torque performance. Consequently, the optimal torque with the maximum value of the objective function will be determined from the database.

The optimization processes of the third and fifth harmonics in the 9-slot/6-pole SPM machine employing the SHC method

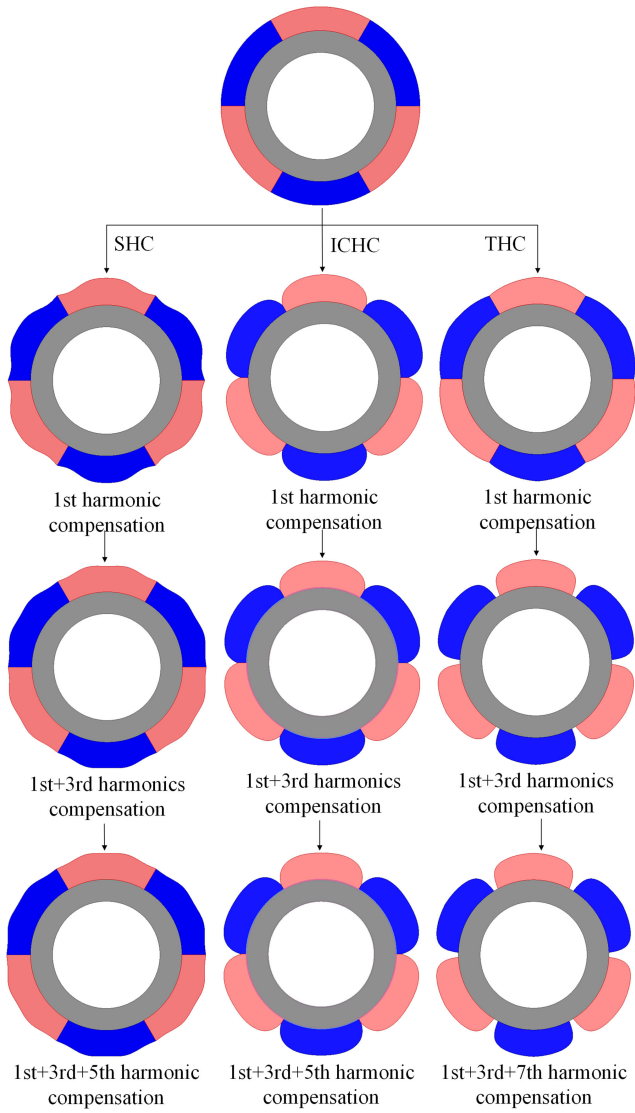


Fig. 7. Shaped SHC, ICHC, and THC rotors with the fundamental, third, fifth, and seventh harmonics compensation.

are given in Figs. 8 and 9, showing the variations of the average torques, the torque ripples and the objective function, with the third and fifth harmonics compensation. As seen from Fig. 8 that the maximum value of the objective function is obtained at  $-0.0892$  where displays the highest average torque and relatively low torque ripple. The fifth harmonic of  $-0.197$  yields the maximum value of the objective function as shown in Fig. 9, resulting from the minimum torque ripple and relatively high average torque. Obviously, the optimal harmonics is determined by the maximum value of the objective function. Besides, the optimization procedures of the ICHC and THC methods are the same to the SHC method. Omitting the detailed process, the optimal values of the fundamental, third, fifth, and seventh

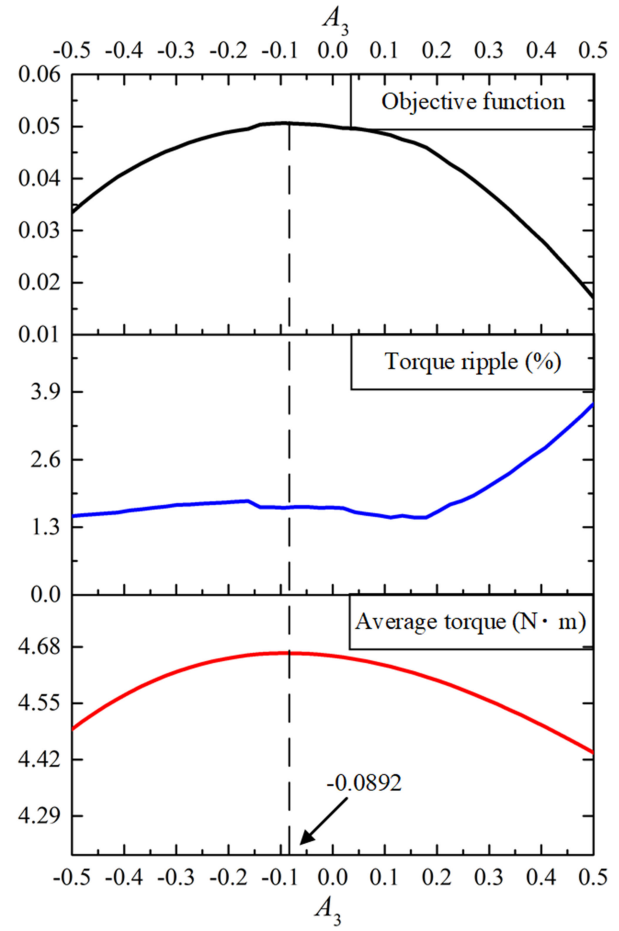


Fig. 8. Variations of average torque, torque ripple, and objective function in 9-slot/6-pole SHC machine with third harmonic  $A_3$  compensation ( $A_1 = 0.529$ ).

harmonics, as well as their corresponding values of the objective function, for the 9-slot/6-pole SPM machine with SHC, ICHC, and THC methods are listed in Table II. Finally, the shaped function of SHC, ICHC, and THC rotors are, respectively, expressed by equation (30) shown at the bottom of this page

$$h'_m(\theta) = 5.5 - 0.628 + 0.529 \sin(1 \times 3\theta) - 0.0892 \sin(3 \times 3\theta) - 0.197 \sin(5 \times 3\theta) \quad (28)$$

$$h'_m(\theta) = 5.5 + 1.59 - 1.5 \div \left\{ \cos \left[ 1 \times \frac{\arccos(\frac{1.5}{5.5})}{0.524} \theta \right] - 0.02 \cos \left[ 3 \times \frac{\arccos(\frac{1.5}{5.5})}{0.524} \theta \right] - 0.04 \cos \left[ 5 \times \frac{\arccos(\frac{1.5}{5.5})}{0.524} \theta \right] \right\} \quad (29)$$

$$h'_m(\theta) = 5.5 + 1.59 - \frac{\sin \left[ \frac{\arctan(2.71-1.5)}{0.524} \theta \right]}{\cos \left[ 1 \times \frac{\arctan(\frac{2.71-1.5}{0.524})}{0.524} \theta \right] + 0.68 \cos \left[ 3 \times \frac{\arctan(\frac{2.71-1.5}{0.524})}{0.524} \theta \right] + 0.012 \cos \left[ 7 \times \frac{\arctan(\frac{2.71-1.5}{0.524})}{0.524} \theta \right]} \quad (30)$$

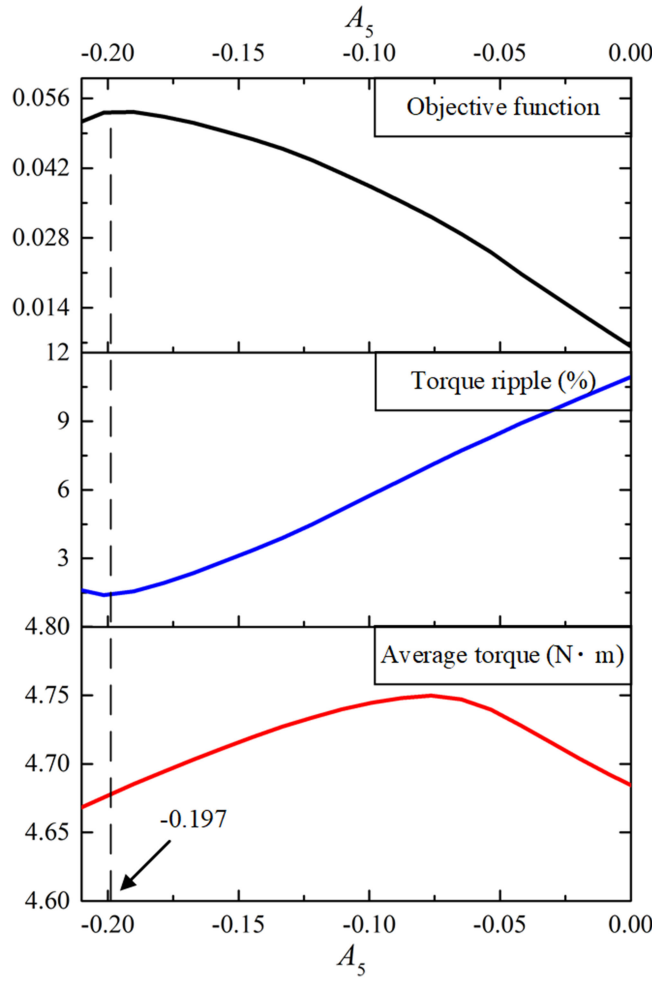


**Fig. 9.** Variations of average torque, torque ripple and objective function in 9-slot/6-pole SHC machine with fifth harmonic  $A_5$  compensation ( $A_1 = 0.529$ ,  $A_3 = -0.0892$ ).

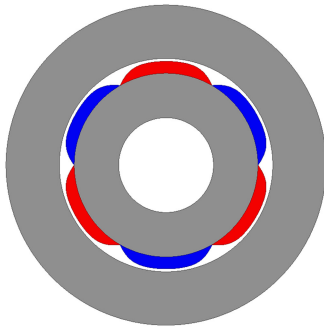


**Fig. 10.** Shaped PM (first+third+fifth harmonics injection) and slotless stator.

#### IV. PERFORMANCE COMPARISONS

To verify the effectiveness of the radial air-gap flux density expression (1), the PM with first+third+fifth harmonics injection and the slotless stator are employed as shown in Fig. 10, and the shaped function is given in (31). The two-dimensional numerical estimation for the magnet with first+third+fifth harmonics

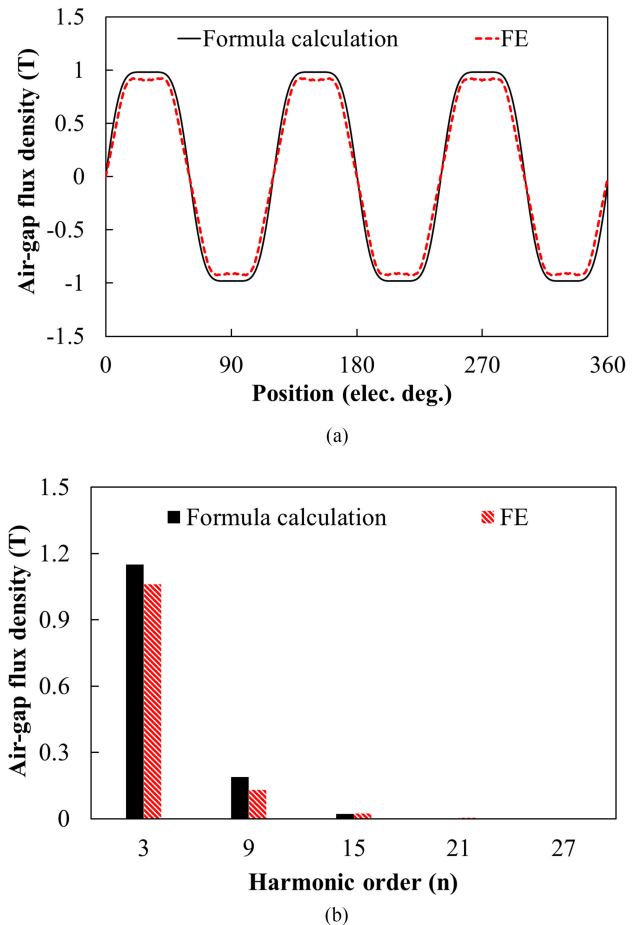


**Fig. 11.** Comparison of FE predicted and formula calculated radial air-gap flux density (first+third+fifth harmonics injection). (a) Waveforms. (b) Harmonics.

injection is given in Fig. 11. The FE predicted waveforms agrees with the formula calculated one as shown in Fig. 11(a), while the amplitudes of FE predicted harmonics are slightly lower than those of the formula calculation as given in Fig. 11(b) due to the flux leakage of the adjacent poles and the presence of the core permeability. Additionally, the tangential component of the resulting flux density is significantly lower than the radial component due to the radial magnetization, thus, ignoring the influence of the tangential component of the flux density.

$$h_m(\theta) = 1.1722 \times 2 \times [\sin(1 \times 3\theta) + 0.1667 \sin(3 \times 3\theta) + 0.0191 \sin(5 \times 3\theta)]. \quad (31)$$

#### A. Comparison of SHC, ICHC, and THC Methods

The harmonic combinations of SHC, ICHC, and THC methods have been listed in Table II. Moreover, the original machine without shaping is added as a reference. The FEM results are summarized in Fig. 12.

Fig. 12(a) shows the air-gap flux density waveforms of the four machines. SHC, ICHC, and THC machines have more sinusoidal flux density waveforms than the original one, and

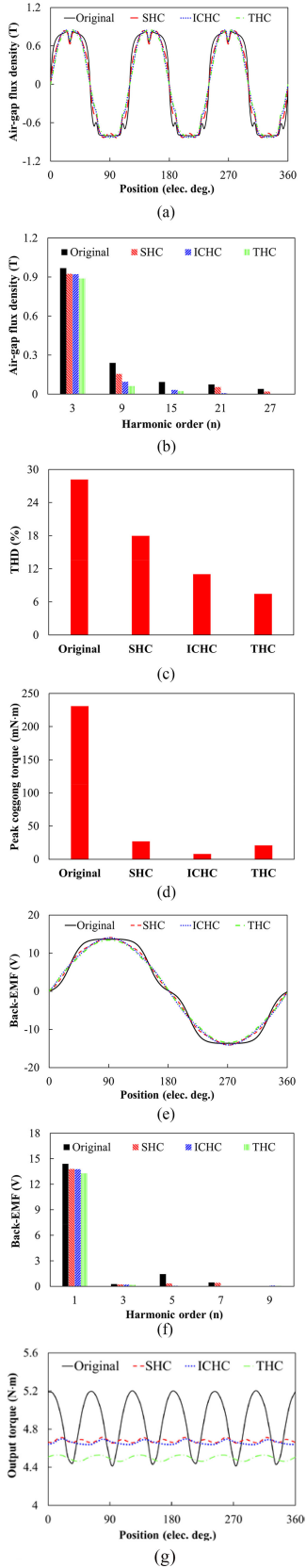


**Fig. 12.** Performance comparisons of 9-slot/6-pole machines with original, SHC, ICHC, and THC rotors. (a) Air-gap flux density waveforms. (b) Air-gap flux density harmonics. (c) THDs of air-gap flux densities. (d) Peak cogging torques. (e) No-load back EMFs. (f) Harmonics of no-load back EMFs. (g) Output torques.

**TABLE III**  
PERFORMANCE COMPARISON OF 9-SLOT/6-POLE SPM MACHINES WITH ORIGINAL, SHC, ICHC, AND THC ROTORS

	Original	SHC	ICHС	THC
Peak current (A)	7.07	7.07	7.07	7.07
Fundamental harmonic of back-EMF (V)	14.4	13.8	13.8	13.3
Peak cogging torque (mN·m)	230.8	26.9	7.9	20.7
PM volume (cm <sup>3</sup> )	54.2	50.4	46.8	43.0
(100%)	(100%)	(93%)	(86%)	(79%)
Average torque (N·m)	4.88	4.68	4.66	4.50
(100%)	(100%)	(96%)	(96%)	(92%)
Ratio of average torque to PM volume (N·m/cm <sup>3</sup> )	0.09	0.093	0.1	0.105
Torque ripple (%)	16.2	1.3	1.2	1.5
Copper loss (W)	61.2	61.2	61.2	61.2
Total core loss (W)	1.35	1.2	1.18	1.1
Eddy loss (mW)	8.4	7.2	5.1	5.8

hence possessing low harmonics. This statement is verified in Fig. 12(b), which presents the air-gap flux density harmonics of the four machines. All rank harmonics of the original machine are highest, and those of the THC machine are lowest. The torque ripple of the THC machine is absolutely small, while the decline of the fundamental harmonic will result in a reduction in the average torque. However, the average torque can be improved by the SHC and ICHC machines, which offer higher fundamental components than the THC machine, and especially the ICHC machine becomes a preferred choice due to the lower third, seventh, and ninth harmonics than the SHC machine. Fig. 12(c) compares the total harmonic distortion (THD) of the four machines. Owing to the lowest harmonic content, the THC machine owns the lowest THD. Additionally, THDs of the SHC and ICHC machines are lower than that of the original machine.

Fig. 12(d) compares the peak cogging torques of the four machines. An extremely low ICHC-machine-based cogging torque can be obtained due to a low THD of air-gap flux density. Although the SHC and THC machines feature higher cogging torques than the ICHC one, the cogging torque is significantly reduced and is lower than that of the original machine. The back EMFs and the harmonic spectrum of the four machines are provided in Fig. 12(e) and (f), respectively. The three shaped machines have more sinusoidal back EMFs than the original machine. Meanwhile, Fig. 12(f) reflects the fact that the SHC, ICHC, and THC machines, with the fundamental, third and fifth harmonics compensation, will not increase any of the undesirable harmonics in the back EMF, compared with the original machine, while improving the back EMF.

Fig. 12(g) compares the output torques of the four machines. The torque ripples of the three shaped machines are much lower than that of the original machine. The results demonstrate that the low cogging torques and sinusoidal back EMFs certainly lead to low torque ripples. However, the average THC-machine-based torque is significantly reduced as compared with that of the original machine. By contrast, the SHC and ICHC machines gain higher average torques than the THC one.

Detailed performances of 9-slot/6-pole original and shaped machines are listed in Table III. Some significant information can be generalized, that is,

**TABLE IV**  
PERFORMANCE COMPARISON OF 9-SLOT/6-POLE SPM MACHINES WITH  
ORIGINAL, SHC, EXISTING I, AND EXISTING II ROTORS

	Original	SHC	Existing I (from [11])	Existing II (from [12])
Peak current (A)	7.07	7.07	7.07	7.07
1st	~	0.529	1	1
3rd	~	-0.0892	1/6	1/6
5th	~	-0.197	~	(3- $\sqrt{5}$ )/40
7th	~	0	~	-0.00052
$\Delta t$ (mm)	~	~	2	2
Average torque (Nm)	4.88	4.68	4.59	4.62
Torque ripple (%)	16.2	1.3	7.3	3.5
Objective function	0	0.054	0.015	0.037

- 1) The three methods are effective for the cogging torque decrement.
- 2) Owing to small THDs and low cogging torques, the torque ripples of shaped machines are reduced by 14.7–15%.
- 3) The fundamental back EMFs of the SHC and ICHC methods decrease slightly, compared with those of the original machines, which avoid a heavy drop in the average torques, while the weakness of the THC method is reflected in the average torque reduction. The average torques of the SHC and ICHC shaped machines occupy 96% of their original machine, and that of the THC shaped machines are only 92% of the original machine.
- 4) The PM volumes of all shaped machines are reduced, and especially that of the THC shaped machines is decreased by 21%. Furthermore, the ratio of the average torque to PM volume is given to illustrate the PM utilization. Considering the case of the severe decrement of PM volume, the THC shaped machines can offer the highest value.
- 5) Compared with the original machine, the eddy loss and the core loss of shaped machines are reduced due to low harmonics of the air-gap flux density.

### B. Comparison of Proposed and Existing Methods

There were many good methods of PM shaping that optimize output torque, and the sine shaping method with third, fifth, and seventh harmonics was investigated to improve the torque. To confirm the effectiveness of the proposed SHC method, the performance comparison of the proposed method and the already presented techniques are examined. The 9-slot/6-pole machines with four topologies for comparison include the original machine, the SHC shaped machine, Existing I of [11] and Existing II of [12]. In addition, the PM edge thickness  $\Delta t$  was optimized to be 2 mm in Existing I and II to compensate the curve effect and flux leakage [10]–[12].

Table IV shows the performances of the four machines. Compared with the original machine, Existing II does not cause a heavy drop in the average torque, while significantly reducing the torque ripple. However, the SHC shaped machine offers higher average torque and lower torque ripple than Existing I and II. Furthermore, the torque quality of the SHC shaped machine is superior to that of Existing I and II in terms of the value of the

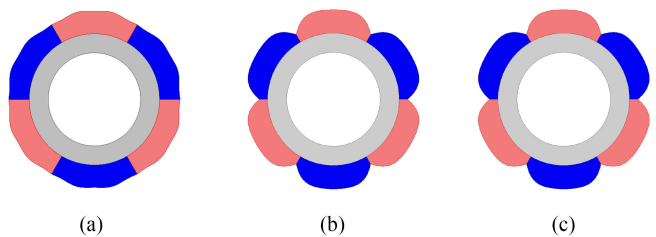


**Fig. 13.** Comparison of SHC and existing rotors. (a) Optimal SHC rotor. (b) SHC rotor with special design parameters ( $\Delta m_a = 3.5$ ,  $A_1 = 4.099$ ,  $A_3 = 0.682$ ,  $A_5 = 0.077$ ,  $A_7 = -0.0038$ ). (c) Rotor of Existing II.

objective function. Therefore, the SHC method shows a priority to existing methods for high-performance servo applications.

In fact, Existing I or Existing II is only one of the SHC rotors, which have been studied in this paper. Fig. 13 compares the SHC and Existing rotors. The optimal SHC rotor absolutely distinguishes from Existing II as shown in Fig. 13(a) and (c), while a SHC rotor with special design parameters, is completely the same to Existing II, as shown in Fig. 13(b) and (c). Hence, the proposed method shows universality in magnet shape design.

Research into inverse cosine function with fundamental and third harmonic injections has been discussed in [14], showing weakness in sufficiently analyzing PM topologies and harmonic combinations, and thus lacking in the universal application for different SPM machines. Furthermore, the result in [14] showed that the optimal third harmonics is 0.167 of the fundamental component to obtain the maximum average torque. Then, the drawback is revealed in Fig. 14, which indicates the variations of the average torque, torque ripple, and objective function, associated with third harmonic compensation. The maximum average torque is determined at -0.167 indeed. However, the torque ripple at -0.167 is unacceptable, and the torque quality is worse from the perspective of the objective function. The third harmonic of -0.02 obviously yields the optimal torque (namely, the maximum value of the objective function) with a very low torque ripple and relatively high average torque.

### V. EXPERIMENTAL VALIDATION AND DISCUSSION

To verify theoretical analyses, the 9-slot/6-pole SHC machine is prototyped as shown in Fig. 15. Fig. 16 exhibits the PM model. PMs with a complex shape, which is mounted on the rotor core, are manufactured by the low-speed wire-cut electrical discharge machining to guarantee the precise processing via the PM. The specification of the manufactured PM is listed in Table V. Fig. 17 presents the experimental platform including the optical-electricity encoder, dc motor, shaft coupling, torque transducer, prototype, and current clamp.

Fig. 18 shows the measured three-phase no-load back EMFs of the prototype, exhibiting a sinusoidal distribution. Analytical calculated no-load back EMFs based on slotless stator and slot stator, as well as the FE predicted and measured results are compared in Fig. 19. The analytical calculated (the slotless stator) fundamental, fifth and seventh harmonics provide the highest

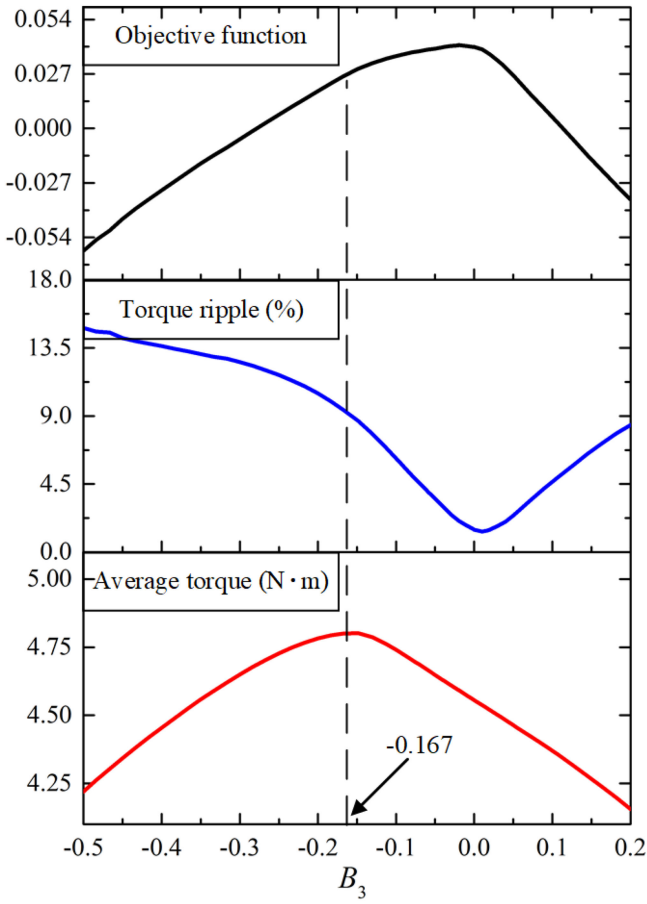


Fig. 14. Variations of average torque, torque ripple, and objective function in 9-slot/6-pole ICHC machine with third harmonic compensation.

TABLE V

SPECIFICATIONS OF MANUFACTURED PM IN 9-SLOT/6-POLE MACHINE

Design parameters	9-slot/6-pole
Magnet remanence $B_r$ and Coercivity	1.21 T and 880 KA/m
Shaped magnet arc	0.0162 rad or 60°
Ratio of shaped arc to pole pitch	1
Maximum height	5.5 mm
Manufacturing tolerance	±0.02 mm
Material of PMs	NdFeB35
Material of stator and rotor	DW465_50
Shaped function (surface profile)	$h'_m(\theta) = 5.5 - 6.44 + 0.529 \sin(1 \times 3\theta) - 0.0892 \sin(3 \times 3\theta) - 0.197 \sin(5 \times 3\theta)$

values due to the absence of considering the slot/teeth effect, the flux leakage and the core saturation. Since the injected harmonics can counteract the effects of slot and teeth, the fifth and seventh harmonics of the analytical calculation (the slot stator) reduces compared with analytical calculated results of the slotless stator. Therefore, the analytical calculated results based on the slot stator match more with the FE predicted results. The fundamental harmonics of the measured and predicted back EMFs are 12.8 and 13.8 V, respectively. Both of their undesirable harmonics are very low, and specifically, their THDs of back EMFs are less than 4.5%.



Fig. 15. Prototype of 9-slot/6-pole SHC machine.

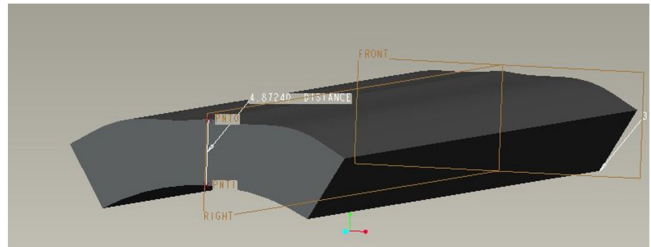


Fig. 16. PM model.

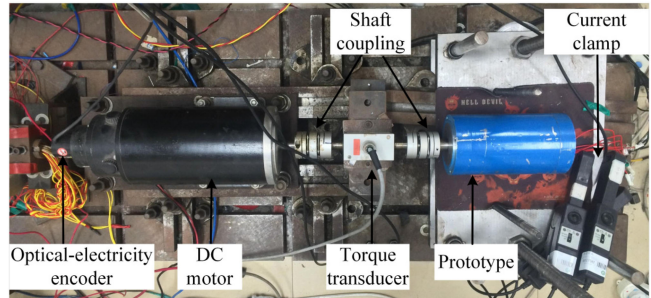


Fig. 17. Experimental platform.

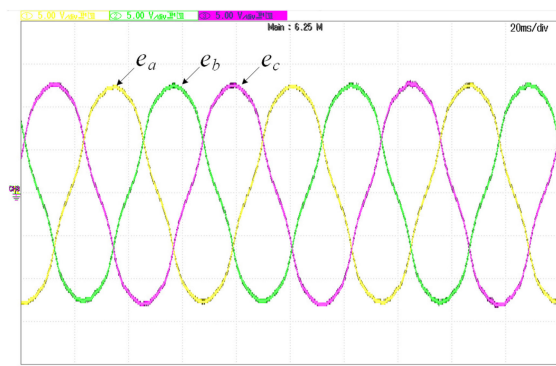
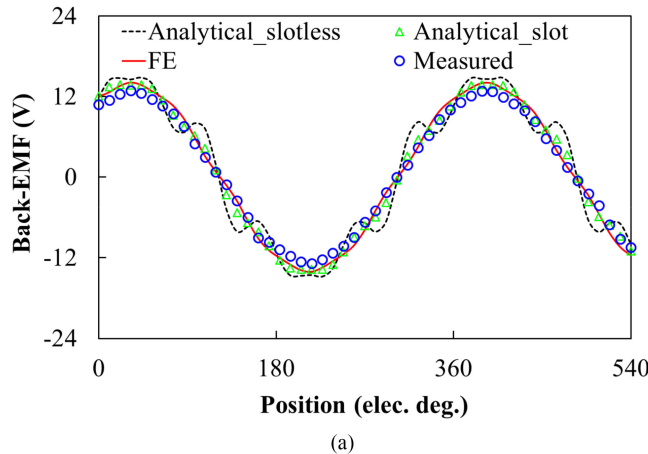


Fig. 18. Measured three-phase no-load back EMFs (300 r/min, 5 V/div).



**Fig. 19.** Comparison of analytical calculated (slotless and slot stators), FE predicted and measured no-load back EMFs. (a) Waveforms. (b) Harmonics.

Since the back EMF of the shaped machine is sensitive to the parameter variation, the measured result would be influenced by the manufacturing tolerance, experimental measurement and other factors. To account the manufacturing tolerance with FEM, the SHC machine with the equivalently manufacturing tolerance of the wire-electrode cutting  $\pm 0.02$  mm (see Table V) is simulated. The shaped function of the SHC machine with the equivalently manufacturing tolerance ( $\pm 0.02$  mm) is given by

$$h'_m(\theta) = 5.5 - 0.628 + 0.529 \sin(1 \times 3\theta) - 0.0892 \sin(3 \times 3\theta) - 0.197 \sin(5 \times 3\theta) \pm 0.02. \quad (32)$$

Comparisons of the original machine, the SHC machine, the SHC machine with the equivalently manufacturing tolerance ( $\pm 0.02$  mm) and the measured machine regarding the back EMF harmonics are given in Fig. 20. The undesirable harmonics of the four shaped machines are much lower than the original machine. Compared with the SHC machine, the fifth harmonics of the SHC machine with equivalently manufacturing tolerance ( $+0.02$  mm) and the measured machine increase, while that of the SHC machine with equivalently manufacturing tolerance ( $-0.02$  mm) reduces. It provides the possibility that the man-

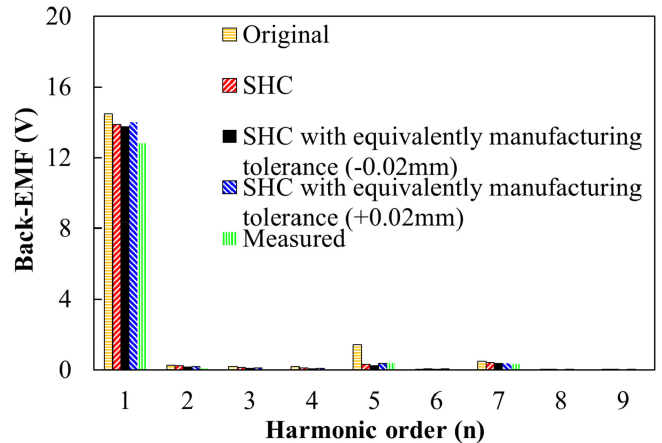


**Fig. 20.** Comparison of original predicted, SHC predicted, SHC with equivalently manufacturing tolerance predicted ( $\pm 0.02$  mm) and measured no-load back EMF harmonics.

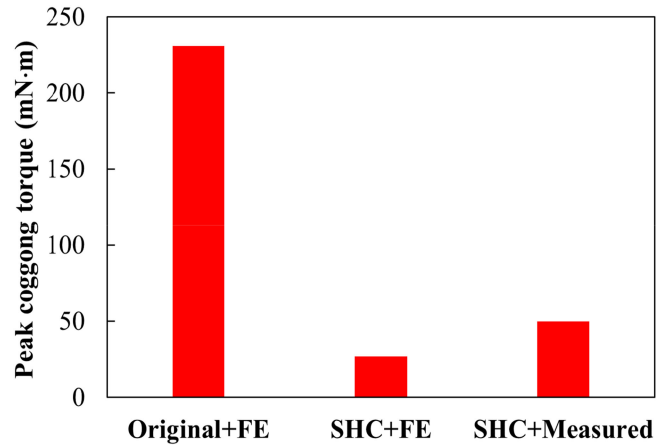


**Fig. 21.** Comparison of measured and FE predicted cogging torques.

factured PM thickness is a litter higher than the FE used. Therefore, it can be speculated that the increase of the fifth harmonic in the measured result may be caused by some aspects like the manufacturing accuracy. On the other hand, the deviation between FE predicted and measured fifth harmonics of the back EMF is an acceptable tolerance and can be ignored

Fig. 21 shows the experimental peak-cogging-torque which is measured by the torque sensor under the case of without power supply. The measured peak-cogging-torque is slightly higher than the predicted, while its value of 50 mN·m should be an acceptable result.

The comparison of the FE predicted and measured output torques is presented in Fig. 22. The average torque (the fundamental harmonic) of the measurement is a little lower than that of the FE prediction, and meanwhile, the measured torque ripple is higher than the FE predicted one. The factors of inducing the measurement errors may include the slightly low magnet remanence of the PM in the experiment, the manufacturing tolerance of wire-electrode cutting, the nonideality of the radial magnetization, and the assembly error of the machine. Fig. 23 compares

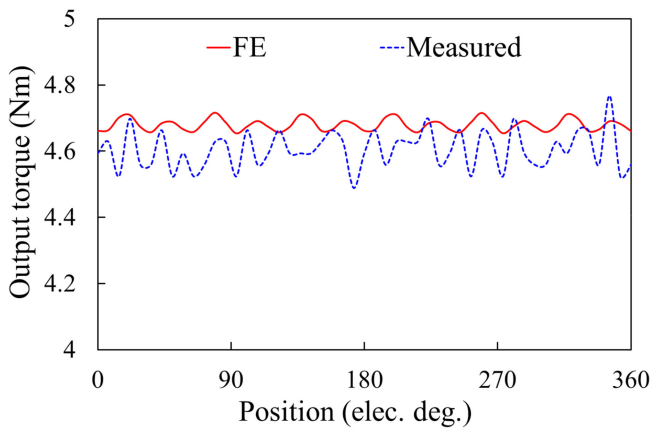


Fig. 22. Comparison of measured and FE predicted output torque waveforms.

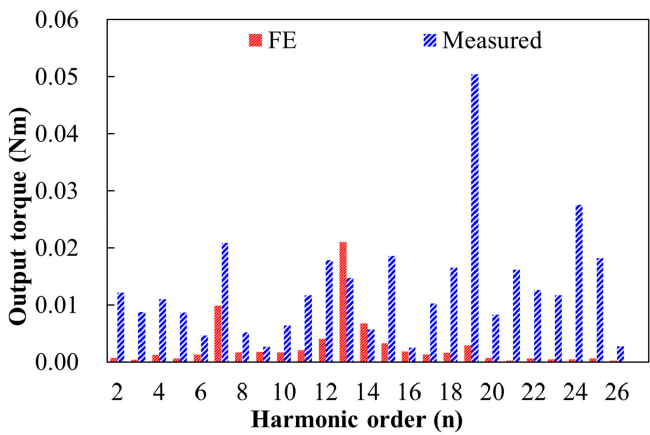


Fig. 23. Comparison of measured and FE predicted output torque harmonics.

measured and FE predicted output torque harmonics, showing that a majority of harmonics of the measured output torque are much higher than that of the FE predicted one, resulting in a higher torque ripple.

## VI. CONCLUSION

In this paper, three new methods to improve torque quality were proposed, including the SHC, ICHC, and THC. A key parameter  $\Delta m$  was introduced to map the relation between varied maximum PM thickness and injected harmonics. Since the SHC and ICHC shaped machines offer high average torques and low torque ripples, they are significantly suitable for the high-performance servo system. The THC machine provides an unconfident average torque, whereas it characterizes a low THD, high PM utilization and small torque ripple under a small workload. Hence, the THC method adapts to the cases of acquiring low torque ripple.

To summarize the findings, the electromagnetic performance of the original and shaped machines were compared, showing that the torque ripples of the SHC and ICHC shaped machines are reduced by 14.9–15% as compared to the original machines,

while their average torques had a loss of 4% under a small PM volume. Finally, a 9-slot/6-pole SHC prototype machine was measured to validate the theoretical analyses.

## REFERENCES

- [1] M. Cheng, L. Sun, G. Buja, and L. Song, "Advanced electrical machines and machine-based systems for electric and hybrid vehicles," *Energy*, vol. 8, no. 9, pp. 9541–9564, Sep. 2015.
- [2] W. P. Cao, B. C. Mecrow, G. J. Atkinson, J. W. Bennett, and D. J. Atkinson, "Overview of electric motor technologies used for more electric aircraft (MEA)," *IEEE Trans. Ind. Electron.*, vol. 59, no. 9, pp. 3523–3531, Sep. 2012.
- [3] M. Cheng and Y. Zhu, "The state of the art of wind energy conversion systems and technologies: A review," *Energy Convers. Manage.*, vol. 88, pp. 332–347, Dec. 2014.
- [4] M. Flankl, A. Tuysuz, and J. W. Kolar, "Cogging torque shape optimization of an integrated generator for electromechanical energy harvesting," *IEEE Trans. Ind. Electron.*, vol. 64, no. 12, pp. 9806–9814, Dec. 2017.
- [5] G. Liu, X. Du, W. Zhao, and Q. Chen, "Reduction of torque ripple in inset permanent magnet synchronous motor by magnets shifting," *IEEE Trans. Magn.*, vol. 53, no. 2, Feb. 2017, Art. no. 8100713.
- [6] Z. S. Du and T. A. Lipo, "Efficient utilization of rare earth permanent-magnet materials and torque ripple reduction in interior permanent-magnet machines," *IEEE Trans. Ind. Appl.*, vol. 53, no. 4, pp. 3485–3495, Jul./Aug. 2017.
- [7] Y. H. Jung, M. S. Lim, M. H. Yoon, J. S. Jeong, and J. P. Hong, "Torque ripple reduction of IPMSM applying asymmetric rotor shape under certain load condition," *IEEE Trans. Energy Convers.*, vol. 33, no. 1, pp. 333–340, Mar. 2018.
- [8] H. Hong and J. Yoo, "Shape design of the surface mounted permanent magnet in a synchronous machine," *IEEE Trans. Magn.*, vol. 47, no. 8, pp. 2109–2117, Aug. 2011.
- [9] Y. Li, J. B. Zou, and Y. P. Lu, "Optimum design of magnet shape in permanent-magnet synchronous motors," *IEEE Trans. Magn.*, vol. 39, no. 6, pp. 3523–3526, Nov. 2003.
- [10] K. Wang, Z. Q. Zhu, and G. Ombach, "Torque improvement of surface mounted permanent-magnet machine using 3rd order harmonic," *IEEE Trans. Magn.*, vol. 50, no. 3, Mar. 2014, Art. no. 8100210.
- [11] K. Wang, Z. Q. Zhu, Y. Ren, and G. Ombach, "Torque improvement of dual three-phase permanent-magnet machine with third-harmonic current injection," *IEEE Trans. Ind. Electron.*, vol. 62, no. 11, pp. 6833–6844, Nov. 2015.
- [12] K. Wang, Z. Y. Gu, Z. Q. Zhu, and Z. Z. Wu, "Optimum injected harmonics into magnet shape in multiphase surface-mounted PM machine for maximum output torque," *IEEE Trans. Ind. Electron.*, vol. 64, no. 6, pp. 4434–4443, Jun. 2017.
- [13] G. Liu, Y. Zeng, W. Zhao, and J. Ji, "Permanent magnet shape using analytical feedback function for torque improvement," *IEEE Trans. Ind. Electron.*, vol. 65, no. 6, pp. 4619–4630, Jun. 2018.
- [14] K. Wang, Z. Q. Zhu, G. Ombach, and W. Chlebosz, "Average torque improvement of interior permanent-magnet machine using 3rd harmonic in rotor shape," *IEEE Trans. Ind. Electron.*, vol. 61, no. 9, pp. 5047–5057, Sep. 2014.
- [15] M. Cheng, P. Han, and W. Hua, "General airgap field modulation theory for electrical machines," *IEEE Trans. Ind. Electron.*, vol. 64, no. 8, pp. 6063–6074, Aug. 2017.



**Yu Zeng** (S'18) received the B.Sc. and M.Sc. degrees in electrical engineering from Jiangsu University, Zhenjiang, China, in 2014 and 2017, respectively. He is currently working toward the Ph.D. degree in electrical engineering with Southeast University, Nanjing, China.

His research interests include the design and analysis of permanent magnet synchronous machines and brushless doubly-fed machines.



**Ming Cheng** (M'01–SM'02–F'15) received the B.Sc. and M.Sc. degrees from the Department of Electrical Engineering, Southeast University, Nanjing, China, in 1982 and 1987, respectively, and the Ph.D. degree from the Department of Electrical and Electronic Engineering, University of Hong Kong, Hong Kong, in 2001, all in electrical engineering.

Since 1987, he has been with the Southeast University, where he is currently a Chair Professor in electrical engineering with the School of Electrical Engineering and the Director of the Research Center for Wind Power Generation. He was a Visiting Professor with the Wisconsin Electric Machine and Power Electronics Consortium, University of Wisconsin-Madison, USA, in 2011 and a Visiting Professor with Aston University, U.K., in 2016–2019. He has authored or coauthored more than 390 technical papers and four books, and is the holder of 120 patents in these areas. His research interests include electrical machines, motor drives for electric vehicle (EV), and renewable energy generation.

Dr. Cheng is currently a Fellow of the Institution of Engineering and Technology. He was the Chair and an Organizing Committee Member for many international conferences. He was a Distinguished Lecturer of the IEEE Industry Application Society in 2015 and 2016.



**Wenxiang Zhao** (M'08–SM'14) received the B.Sc. and M.Sc. degrees from Jiangsu University, Zhenjiang, China, in 1999 and 2003, respectively, and the Ph.D. degree from Southeast University, Nanjing, China, in 2010, all in electrical engineering.

Since 2003, he has been with Jiangsu University, where he is currently a Professor in electrical engineering with the School of Electrical Information Engineering. From 2008 to 2009, he was a Research Assistant with the Department of Electrical and Electronic Engineering, University of Hong Kong, Hong Kong. From 2013 to 2014, he was a Visiting Professor with the Department of Electronic and Electrical Engineering, University of Sheffield, Sheffield, U.K. He has authored and coauthored more than 130 technical papers in these areas. His current research interests include electric machine designs, modeling, fault analysis, and intelligent control.



**Guohai Liu** (M'07–SM'15) received the B.Sc. degree from Jiangsu University, Zhenjiang, China, in 1985, and the M.Sc. and Ph.D. degrees from Southeast University, Nanjing, China, in 1988 and 2002, respectively, all in electrical engineering and control engineering.

Since 1988, he has been with Jiangsu University, where he is currently a Professor in electrical engineering, the Dean of the School of Electrical Information Engineering. From 2003 to 2004, he was a Visiting Professor with the Department of Electronic and Electrical Engineering, University of Sheffield, Sheffield, U.K. He has authored or coauthored more than 200 technical papers and four textbooks, and holds 30 patents in these areas. His research interests include electrical machines, motor drives for electric vehicles and intelligent control.